


[View Journal Online](#)
[View Article Online](#)

Indirect detection of 5-hydroxytryptamine and tyramine by using *tris*(2,2'-bipyridyl)ruthenium-graphene modified electrode coupled with capillary electrophoresis

 Zi Wei Zhao , Fan Lin Li  and Ming Su *

Key Laboratory of Analytical Science and Technology of Hebei Province, College of Chemistry and Environmental Science, Hebei University, Baoding, 071002, P. R. China

410690791@qq.com (Z.W.Z.), lifanlinhb@126.com (F.L.L.), suminghbu@126.com (M.S.)

* Corresponding author at: Key Laboratory of Analytical Science and Technology of Hebei Province, College of Chemistry and Environmental Science, Hebei University, Baoding, 071002, P. R. China.

Tel: +86.312.5079739 Fax: +86.312.5079739 e-mail: suminghbu@126.com (M. Su).

RESEARCH ARTICLE

ABSTRACT



doi: 10.5155/eurjchem.10.4.336-344.1852

Received: 22 March 2019

Received in revised form: 15 May 2019

Accepted: 01 September 2019

Published online: 31 December 2019

Printed: 31 December 2019

KEYWORDS

 Graphene
 Tyramine
 5-Hydroxytryptamine
 Electrochemical sensor
 Capillary electrophoresis
 Electrochemiluminescence

A highly sensitive and stable solid-state electrochemiluminescence (ECL) sensor was developed based on *tris*(2,2'-bipyridyl)ruthenium(II) ($\text{Ru}(\text{bpy})_3^{2+}$) integrating with 2,2'-azino-bis(3-ethylbenzothiazoline-6-sulfonic acid) (ABTS) functionalized graphene. $\text{Ru}(\text{bpy})_3^{2+}$ is incorporated with the ABTS functionalized graphene based on not only the π - π stacking but also electrostatic interactions. Coupled with capillary electrophoresis (CE), this ECL sensor was used to detect tyramine and 5-hydroxytryptamine (5-HT) based on their quenching effects for the $\text{Ru}(\text{bpy})_3^{2+}$ /tripropylamine (TPA) system. The quenching mechanism was illustrated and the conditions for CE separation and ECL detection were optimized. Based on an $S/N = 3$, the limit of detection (LOD) for tyramine and 5-HT were 0.1 μM and 0.02 μM , respectively. The applicability of the proposed method was further illustrated in the determination of tyramine and 5-HT in human plasma samples from small intestine carcinoid patients.

 Cite this: *Eur. J. Chem.* 2019, 10(4), 336-344

 Journal website: www.eurjchem.com

1. Introduction

Electrogenerated chemiluminescence is the process where species generated at electrodes undergo high-energy electron-transfer reactions to form excited states, as a luminophore, to emit light [1]. Among many ECL reagents, *tris*(2,2'-bipyridyl)ruthenium(II) ($\text{Ru}(\text{bpy})_3^{2+}$) and its derivatives have received considerable attention thanks to some of their advantages [2,3]. Since the first report of ECL of $\text{Ru}(\text{bpy})_3^{2+}$ by Tokel and Bard in 1972 [4], related researches have been proliferated. Nowadays, the $\text{Ru}(\text{bpy})_3^{2+}$ ECL technique has become a powerful analytical tool and has been widely used in the areas of immunoassay [5], clinic diagnosis [6-8], food and water testing [9], biowarfare agent monitoring [10], as well as DNA hybridization detection [11]. $\text{Ru}(\text{bpy})_3^{2+}$ ECL has also been exploited for analytical application by combining with different separation techniques such as capillary electrophoresis, microchip electrophoresis (ME), and high performance liquid chromatography (HPLC). Especially, $\text{Ru}(\text{bpy})_3^{2+}$ ECL system coupled with CE has been widely studied due to its important applications in separation and determination of different

compounds that contained amino acids, alkyl amines, and pharmaceuticals [12,13]. However, in the vast majority of reports, $\text{Ru}(\text{bpy})_3^{2+}$ was directly added in the cathodic cell, and this post-column addition mode is facing some problems. For example, the CE buffer flowed from the capillary can dilute the concentration of $\text{Ru}(\text{bpy})_3^{2+}$ near the surface of the working electrode. The other shortcoming of the static storage mode is the excessive consumption of $\text{Ru}(\text{bpy})_3^{2+}$.

To solve these problems, immobilization of $\text{Ru}(\text{bpy})_3^{2+}$ on the electrode is expected to be an effective method. Great efforts have been made toward the immobilization of $\text{Ru}(\text{bpy})_3^{2+}$ on a solid electrode surface as a means to reduce the consumption of expensive reagents, simplify experimental design and to create a re-generable sensor [14,15]. Examples of some approaches include the incorporation of $\text{Ru}(\text{bpy})_3^{2+}$ molecules into ion exchange polymer (e.g., Nafion, Eastman AQ55D) composite films through electrostatic attachment, covalently embedded into sol-gel-based composite films, layer-by-layer self-assembly and the Langmuir-Blodgett technique [16].

Graphene (G) is a new type of carbon material with a two-dimensional honeycomb lattice and single-atom-thick sheet carbon atom that has recently attracted much attention due to its unique optical, thermal and electrochemical properties [17,18]. Especially, the graphene sheets show fast electron transfer kinetics and excellent electrocatalytic characteristics compared with graphite and glassy carbon. It has been shown to be excellent platform for non-covalent and covalent functionalization [19]. Of particular interest for us is to exploit its application in the field of electrochemistry and film-forming properties. In order to increase the charge density on the graphene sheets, 2,2-azino-bis(3-ethylbenzothiazoline-6-sulfonic acid) are assembled onto a graphene surface. Moreover, ABTS was also as a stabilizer to prevent the irreversible agglomerates or restack to form graphite through strong π - π stacking and van der Waals interaction [20]. Recently, the ABTS-graphene composite films were used to immobilize enzyme molecules for designing a novel biosensing platform [21].

In the present study, we described a new immobilization approach by attaching $\text{Ru}(\text{bpy})_3^{2+}$ to ABTS functionalized graphene via electrostatic and π - π stacking interaction. The electron-rich ABTS molecule stacked on the surface of graphene through π - π electronic interactions can not only improve the stability but also increased negative charge density of graphene, which is advantage to the interaction between $\text{Ru}(\text{bpy})_3^{2+}$ and graphene. This stable solid-state ECL sensor was applied as detector to analyze two catecholamine neurotransmitters in plasma samples based on quenching $\text{Ru}(\text{bpy})_3^{2+}$ /tripropylamine (TPA) ECL by coupling with CE. Also, the quenched ECL reaction mechanisms of $\text{Ru}(\text{bpy})_3^{2+}$ /TPA system were investigated in the presence of 5-HT and tyramine. Other experimental conditions for the separation and simultaneous detection of 5-HT and tyramine were optimized.

2. Experimental

2.1. Reagents and chemicals

Graphite powder (99.99995%, 325 mesh) was obtained from Xian Feng Nano Inc (Nanjing, China). 2,2-Azino-bis(3-ethylbenzothiazoline-6-sulfonic acid) (ABTS) and *tris*(2,2'-bipyridyl)ruthenium(II) chloride hexahydrate ($\text{Ru}(\text{bpy})_3\text{Cl}_2 \cdot 6\text{H}_2\text{O}$) were purchased from Sigma-Aldrich (St. Louis, MO, USA). 5-Hydroxytryptamine and tyramine were purchased from the National Institute for the Control of Pharmaceutical and Biological Products (Beijing, China). The blank plasma samples of colorectal cancer patients as gifts were collected from BenQ Hospital (Nanjing, China). All other reagents used were commercially available and of analytical grade. All solutions were prepared with double distilled water. Phosphate buffer solution (PBS) was made from Na_2HPO_4 and NaH_2PO_4 . Prior to CE analysis, the required sample solutions and PBS were filtered through 0.22 μm cellulose acetate membrane filters (Shanghai Xinya Purification Material Factory, Shanghai, China).

2.2. Apparatus

The FT-IR spectrum was recorded on a Nexus 670 FT-IR spectrophotometer (Nicolet Instruments). Transmission electron microscopy (TEM) images were obtained with a JEOL-2010 transmission electron microscope operating at an accelerating voltage of 120 kV. Tapping mode atomic force microscopy (AFM) characterizations were conducted on an Agilent 5500 atomic force microscopy (Agilent, USA). All separation and detection were done on a Model MPI-A CE-ECL analyzer systems (Xi'an Remax Electronic High-Tech Ltd, Xi'an, China). A programmable high-voltage power supply (0-20 kV)

was applied to drive the electrokinetic sample injection and electrophoretic separation. All data were accomplished with a multifunctional chemiluminescence analyzer, an electrochemical potentiostat and obtained by the MPI-A analysis software. Electrochemical and electrochemiluminescent measurements were performed with a three-electrode system comprising a platinum wire as auxiliary electrode, an Ag/AgCl (saturated KCl) electrode as reference electrode and the ABTS-graphene- $\text{Ru}(\text{bpy})_3^{2+}$ composite modified graphite disk electrode as working electrode. Capillary electrophoresis was performed by using a 35 cm length of uncoated fused-silica capillary (375 μm o.d. 25 μm i.d., Yongnian Optical Fiber Factory, Hebei, China) at 15 kV.

2.3. Synthesis of graphene

Graphene was prepared through a route involving the steps of graphite oxidation, exfoliation, and chemical reduction. Firstly, the process of graphite oxidation was done by Hummer's method with some modification [22,23]. The detailed preparation process used in this work had been reported in our group's paper [24]. Then, the resulting graphite oxide dispersion was used to prepare exfoliated GO. Exfoliation was achieved by sonicating graphite oxide dispersion under ambient conditions for 5 h. At last, the homogeneous yellow-brown suspension was obtained and further used for reduction by hydrazine. The reduction reaction was carried out by adding hydrazine (1.2 mL) into the prepared suspension. After being sonicated for 1 h and kept stirring for 24 h at 50 °C, graphene sheets were obtained by filtration of the product and drying in vacuum.

2.4. Preparation of the $\text{Ru}(\text{bpy})_3^{2+}$ solid sensor

Typically, graphene sheets (10 mg) were dispersed into 1 mL PBS containing 5 mM ABTS and the mixture were stirred for 30 min to prepare ABTS-G composite solution. The composite solution can be stable for several weeks, which indicates the strong stabilizing abilities of the ABTS for graphene. The reason was that ABTS can interact with the graphene surface through π - π electronic interactions. Then the ABTS-G was collected by centrifugation for 20 min. The supernatant was removed, and ABTS-G was thoroughly washed at least thrice with water to remove the loosely adsorbed ABTS. Next, the planer positively charged $\text{Ru}(\text{bpy})_3^{2+}$ was assembled on the surface of negatively charged ABTS-G via the electrostatic interaction and π - π stacking interaction by stirring ABTS-G (5 mg) and $\text{Ru}(\text{bpy})_3^{2+}$ (10 mM) in pH = 7.5 PBS at room temperature for 2 h. After that, the mixture was centrifuged and the $\text{Ru}(\text{bpy})_3^{2+}$ -ABTS-G hybrid was collected by removing the supernatant. The hybrid was washed with PBS to remove the loosely assembled $\text{Ru}(\text{bpy})_3^{2+}$ molecules.

To fabricate the solid-state ECL sensor, the bare electrode was pretreated to make sure clean enough before being modified. Then, 10 μL $\text{Ru}(\text{bpy})_3^{2+}$ -ABTS-G hybrid suspension (2 mg/mL) was dipped onto the surface of the pretreated graphite disk electrode. The solvent was allowed to be evaporated at ambient temperature under atmosphere before use. The $\text{Ru}(\text{bpy})_3^{2+}$ -ABTS-G modified electrode was stored at room temperature when not in use.

2.5. Preparation of plasma sample

About 2 mL of anticoagulant human blood was collected in a 5 mL centrifuge tube and centrifuged at 12000 rpm for 10 min. The supernatant collected in a 1.5 mL micro centrifuge tube was detected immediately. These samples were diluted to 5-fold with 10 mM pH = 7.4 PBS, and then filtrated through a 0.22 μm cellulose acetate membrane before CE analysis [25,26].

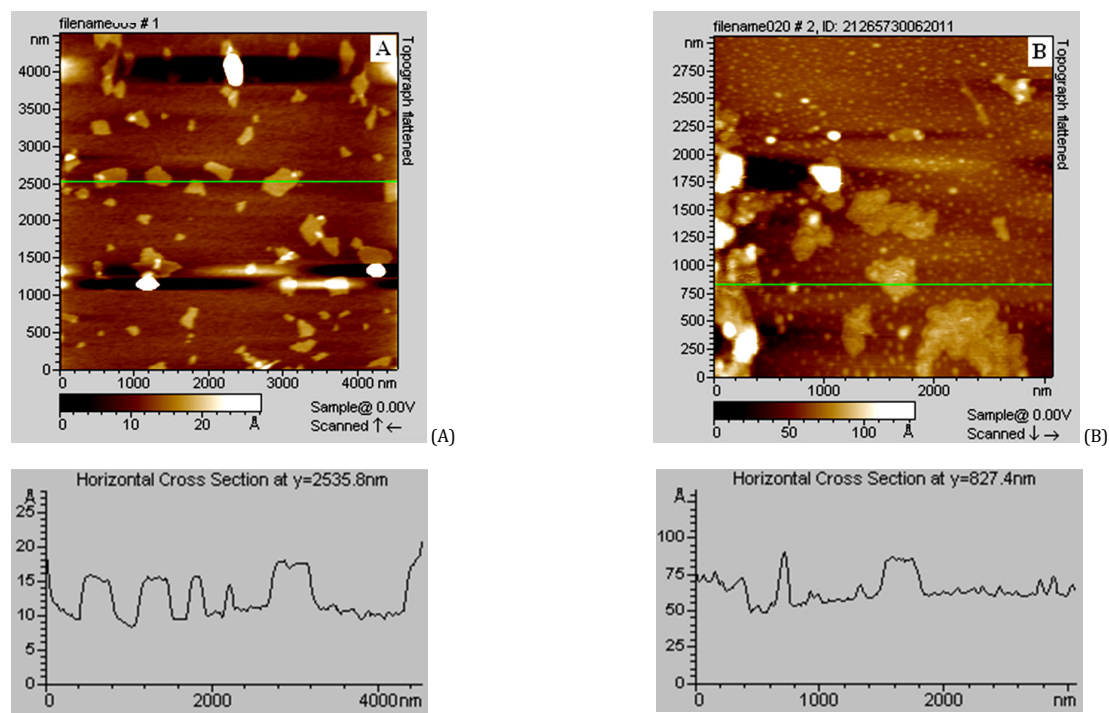


Figure 1. Typical tapping mode AFM images and the cross-sectional analysis of graphene sheets without (A) and with (B) assembly of ABTS and Ru(bpy)₃²⁺.

2.6. Electrophoresis procedure

The new capillary was filled with 0.1 M NaOH over night before use. Prior to starting a series of analyses, the capillary was washed with 1.0 M NaOH for 5 min, followed by double distilled water for 5 min, and equilibrated with the running buffer for 5 min to maintain an active and reproducible inner surface. During the experiment, separation voltage (15 kV) was applied across the capillary, and the detection potential (1.20 V versus Ag/AgCl) was applied at the working electrode. When the system was used to separate and detect the 5-HT and tyramine, the separation buffer in the experiment was 15 mM PBS at pH 8.5 containing 0.5 mM TPA and the detection buffer in the ECL cell was 50 mM PBS at pH = 8.0. The immobilized Ru(bpy)₃²⁺ electrode was aligned with the separation capillary with a distance of about 75 μm. Electromigration injection (10 kV×10 s) was used for sample introduction.

3. Results and discussion

3.1. Characterization of G and functionalized G Conjugate

Functionalized graphene together with the original graphene was first characterized by AFM. As shown in Figure 1A, the cross-sectional analysis indicates that the thickness of most graphene is ca.0.6 nm which matches well with the reported apparent thickness of graphene sheets [20,27,28], suggesting the single-sheet graphene was obtained in this work. However, this value is still somewhat larger than the theoretical thickness for a perfectly flat sp²-carbon-atom network (ca. 0.3 nm), which could be attributed to the residual oxygen functionalities on graphene [29]. The AFM image also reveals the morphology and distribution of graphene nanostructure is uniform, which is beneficial to improve the loading amount of Ru(bpy)₃²⁺ and accelerate electron transfer. After the assembly of Ru(bpy)₃²⁺, the thickness of the functionalized graphene has a significant increase, up to 2.5-3.0 nm (Figure 1B). This was due to the multilayer adsorb of

Ru(bpy)₃²⁺ whose molecular diameter is 1.08 nm [30]. Because the surface charge density of ABTS modified graphene is higher, more cationic Ru(bpy)₃²⁺ are bound to graphene by electrostatic interaction or strong π-π stacking interaction.

The assembly of ABTS functionalized graphene was also proved by FT-IR spectroscopy. The results suggested that ABTS has been effectively assembled on the surface of graphene. The detailed data were showed in the Supporting Information (Figure S1).

To obtain further information on the structure and topology of graphene and functionalized graphene, the morphologies were further examined by TEM. Figure 2A shows the typical TEM image of graphene. They are transparency, wrinkled with occasional folds and rolled edges. Figure 2B showed that the ABTS modified graphene could serve as a template for orderly decorating with Ru(bpy)₃²⁺ agglomerates via electrostatic and π-π stacking interactions. The attached Ru(bpy)₃²⁺ had a well-scattered distribution on the supports.

3.2. Electrochemistry and ECL behavior of the solid-state ECL sensor

The electrochemical behavior of Ru(bpy)₃²⁺ immobilized on the solid-state ECL sensor was firstly studied in 0.1 M pH = 8.0 PBS using cyclic voltammetry. Figure 3 showed cyclic voltammograms obtained at a bare electrode (a), a pure graphene-modified electrode (b), and a Ru(bpy)₃²⁺-ABTS-G composite film-modified electrode (c). Similar to that obtained at a bare electrode, the cyclic voltammogram of the pure graphene-modified electrode did not show any observable redox peak, indicating that graphene cannot undergo the redox reaction in the experimental potential ranges. However, its peak current was enhanced because of the excellent electrical conductivity of graphene. The cyclic voltammetric response of the Ru(bpy)₃²⁺-ABTS-G composite modified electrode was characterized by a well-defined oxidation peak at 0.55 V. This peak potential is similar to those for the oxidation of ABTS adsorbed on the surface of carbon nanotubes [31].

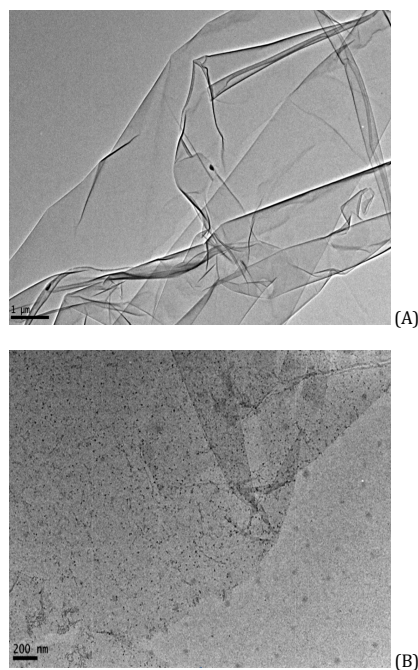


Figure 2. Typical TEM image of graphene (A) and high resolution TEM image of Ru(bpy)₃²⁺-ABTS functionalized graphene sheet (B).

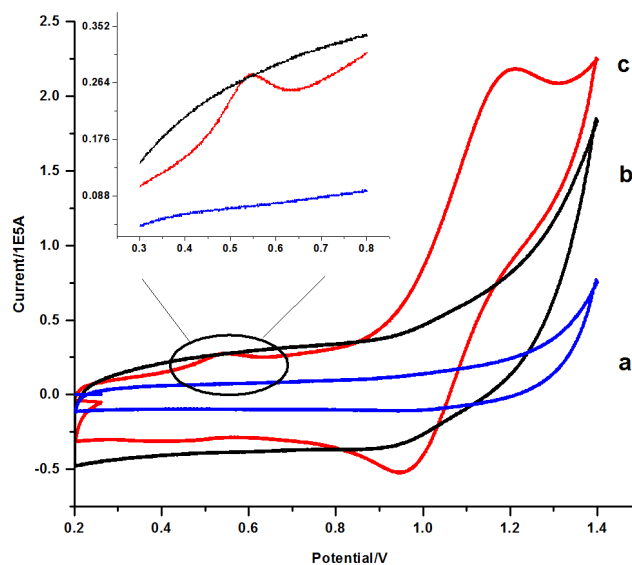


Figure 3. Cyclic voltammograms in 100 mM PBS at pH = 8.0 at a bare electrode (a), a pure graphene-modified electrode (b), and Ru(bpy)₃²⁺-ABTS-G composite film-modified electrode (c) with a scan rate of 100 mV/s.

This result also indicates ABTS was successfully stacked on graphene. Beside this, a pair of redox current peaks of Ru(bpy)₃²⁺, the anodic and cathodic peak potential at 1.20 V and 0.95 V respectively, were also observed. This result also indicated the formation of Ru(bpy)₃²⁺-ABTS-G hybrid, which was in agreement with results that obtained from the spectroscopic method.

3.3. The electrochemical and ECL behavior of the solid-state ECL sensor with TPA as a co-reactant

Figure 4 showed cyclic voltammograms of Ru(bpy)₃²⁺ immobilized on the solid-state ECL sensor in the absence (a) and presence (b) of 50 μM TPA in 100 mM PBS at pH = 8.0. The presence of TPA caused the anodic peak current to increase clearly while the cathodic peak current decreased, consistent

with an electrocatalytic reaction mechanism (Figure 4A). The corresponding ECL-potential profile in the absence (a) and presence (b) of 50 μM TPA during the cyclic voltammetric scan was shown in Figure 4B. The onset of luminescence occurred near 1.0 V and then the ECL intensity rose steeply until it reached a maximum near 1.15 V, which was consistent with the oxidation potential of Ru(bpy)₃²⁺. This means that the oxidation of immobilized Ru(bpy)₃²⁺ plays a key role in the process of ECL. The ECL response of the solid-state sensor was very fast due to the excellent electrical conductivity of graphene.

This ECL sensor was quite stable. Under continuously CV scanning for 500 s with the scan rate of 100 mV/s, there was no apparent change for ECL intensity as demonstrated in Figure 5.

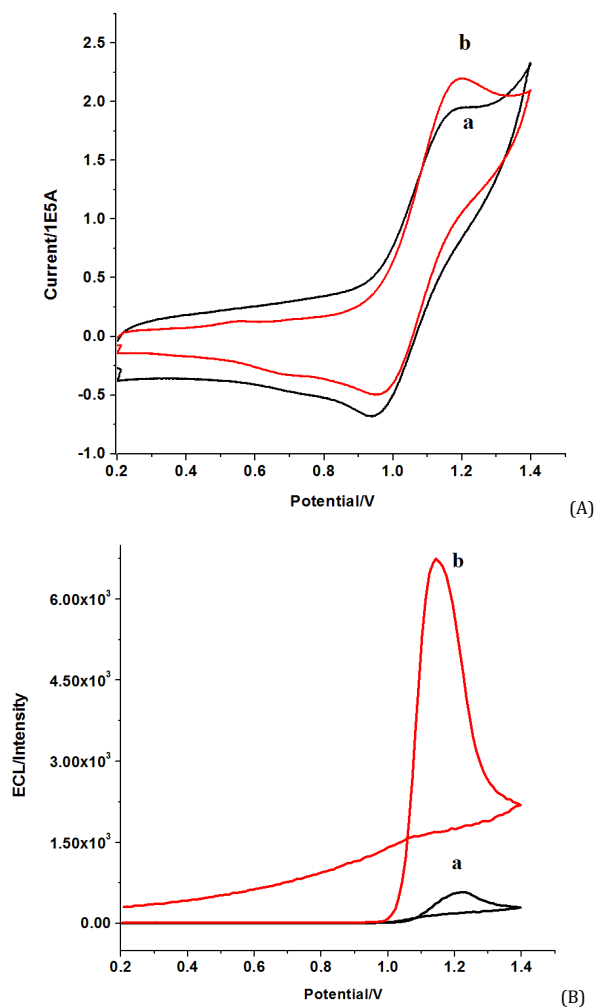


Figure 4. Cyclic voltammograms (A) and corresponding ECL-potential curves (B) of the solid ECL sensor in the absence (a) and presence (b) of 50 μM TPA in 100 mM PBS (pH = 8.0) at a scan rate of 100 mV/s.

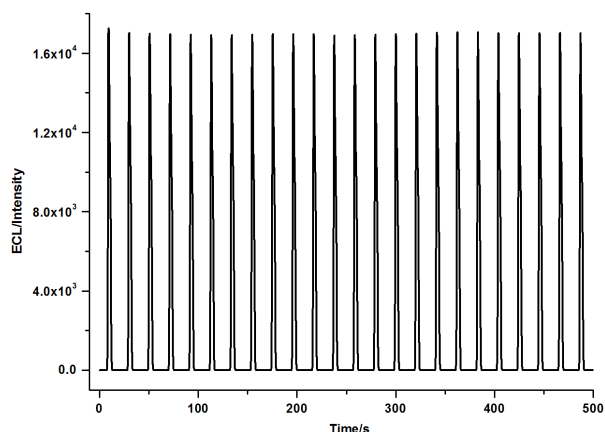


Figure 5. ECL emission from the solid ECL sensor in the presence of 100 μM TPA in 100 mM PBS at pH = 8.0 under continuous CVs for 500 s at a scan rate of 100 mV/s.

The good stability of the ECL sensor may be attributed to the two different kinds of interactions: the strong electrostatic interaction and π - π stacking interactions between positively charged $\text{Ru}(\text{bpy})_3^{2+}$ and negatively charged ABTS functionalized graphene. This indicated that the solid-state ECL sensor also has potential application for CE and microchip electrophoresis on column detection.

3.4. ECL of solid-state sensor in the presence of TPA quenched by tyramine and 5-HT

Figure 6 corresponded to the quenched ECL spectra from immobilized $\text{Ru}(\text{bpy})_3^{2+}$ /TPA system in the potential range of 0.90-1.25 V after adding tyramine and 5-HT as quenchers. In the absent of the quenchers, the strongest ECL emissions appeared at the potential of 1.15 V (Figure 6a).

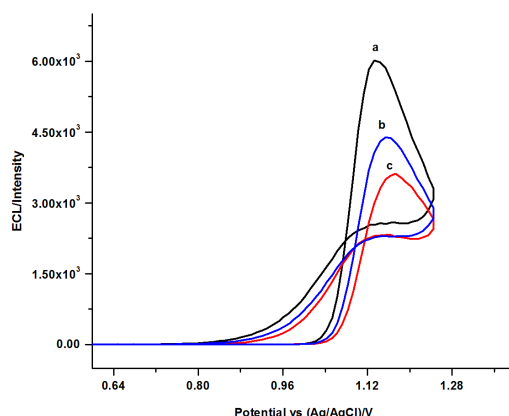
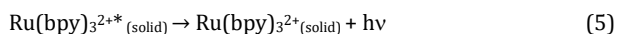
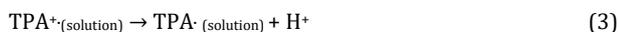
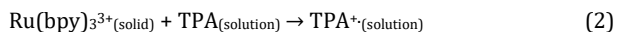
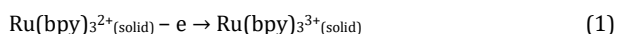


Figure 6. ECL-potential curves of Ru(bpy)₃²⁺ modified electrode in 50 mM PBS at pH = 8.5 containing 50 μM TPA (a), 50 μM TPA with 50 μM tyramine (b), 50 μM TPA with 50 μM 5-HT.

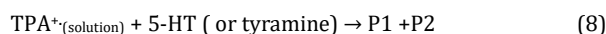
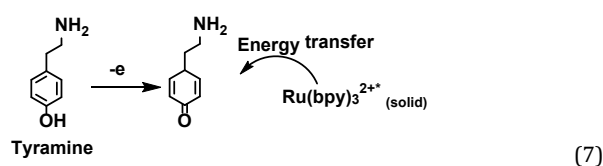
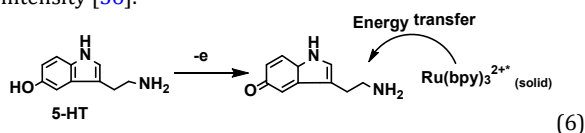
However, the ECL intensity decreased obviously after adding either tyramine (Figure 6b) or 5-HT (Figure 6c). Approximately 30 and 42% of ECL signals were quenched by 50 μM tyramine and 5-HT, respectively. It is known that ECL of Ru(bpy)₃²⁺ systems include electron transfer and deprotonation procedures. ECL intensities relies much on the electron transfer process of Ru(bpy)₃²⁺. Both co-reactants (e.g. TPA) and quenchers (e.g. tyramine and 5-HT) affect the electron transfer process dramatically, resulting in change of the ECL intensity.

3.5. Mechanism discussion

Mechanism for our immobilized Ru(bpy)₃²⁺/TPA system was proposed based on our experimental results and literature suggestions [32]. During the electrochemical oxidation process, the immobilized Ru(bpy)₃²⁺ can be oxidized directly to form Ru(bpy)₃³⁺ (Equation 1) which further oxidized TPA to form TPA radical cation (TPA^{•+}) (Equation 2). TPA^{•+} is unstable and short-lived, and is believed to lose a proton from an α-carbon to form the strongly reducing intermediate TPA⁻ (Equation 3). This reducing intermediate was then reacted with Ru(bpy)₃³⁺ via an electron transit reaction to generate emitting species of Ru(bpy)₃^{2+*} (Equation 4).



When tyramine or 5-HT was added, phenol groups were oxidized electrochemically to benzoquinone (Equations 6 and 7) which can quench excited states of transition-metal complexes via energy transfer [33-35]. Therefore, in our experiment the quenching is believed to occur via energy transfer from *Ru(bpy)₃²⁺ to benzoquinone. In the meantime, the quenchers react with TPA intermediate radicals (Equation 8), which rapidly consumes TPA^{•+} and decreases the ECL intensity [36].



The ECL intensity was related closely to the 5-HT or tyramine concentration. The quenching behavior can be described by the Stern-Volmer equation [37]

$$I_0/I = 1 + K_{SV}[Q] \quad (9)$$

where I_0 and I define the ECL intensities in the absence and presence of the quencher, respectively. The Stern-Volmer constant, K_{SV} , represents the efficiency of quenching. From the Stern-Volmer plot shown in Figure 7, the value of K_{SV} for the quenching of Ru(bpy)₃²⁺ ECL by 5-HT and tyramine were calculated to be 2.29×10^4 and $1.37 \times 10^4 \text{ M}^{-1}$, respectively.

3.6. Optimization of detection conditions

Ru(bpy)₃²⁺ modified electrode was used as a solid-state ECL detector in CE for separating and detecting 5-HT and tyramine. The concentration of TPA in CE running buffer was optimized (Figure S2). Results showed that increase of the TPA concentration resulted in enhancement of the quench efficiency for both 5-HT and tyramine. However, too high TPA concentrations led to strong background noises and thus, the low S/N value. Thus, 0.6 mM TPA as buffer additive was added in subsequent experiments.

Figure S3 showed the ECL intensity as a function of the potential applied on the working electrode (from 1.10 to 1.35 V). As increase of applied potential, the quenched ECL intensity for both 5-HT and tyramine increased and reached a maximum value at 1.20 V. When the potential exceeded 1.20 V, the quenched ECL responses markedly decreased, possibly resulted from the negative effect of the oxidation of water. Furthermore, too high potentials also led to huge background noises and an unstable baseline.

The step of deprotonating to form free intermediates for amines is critical to the intensity of Ru(bpy)₃²⁺/TPA ECL system, and this course is sensitive to solution pH value. Effects of pH value ranging from 6.5 to 9.5 in detection cell on quench efficiency of the two analytes and the ECL background signal intensity were investigated. (Figure S4). Quench efficiency reached a maximum value at pH = 8.0.

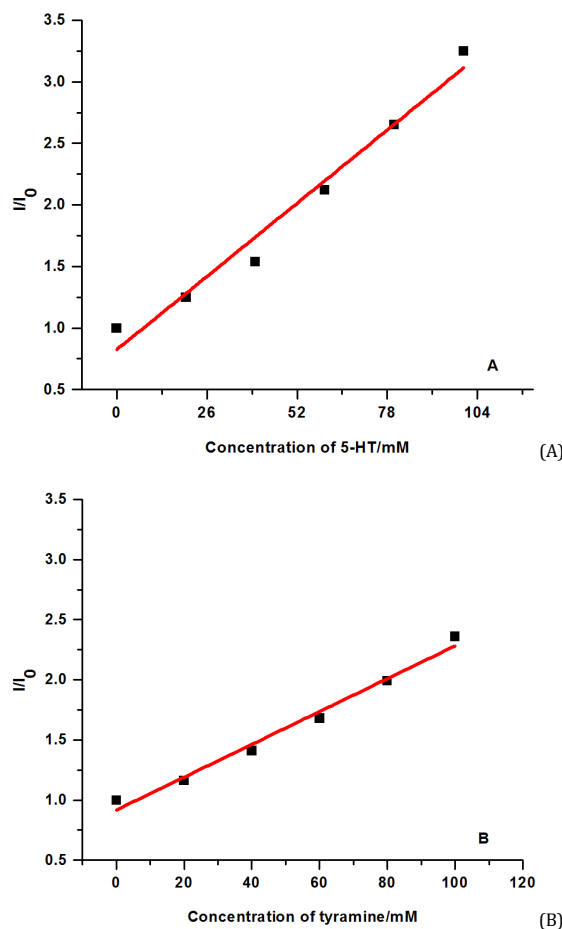


Figure 7. Stern-Volmer ECL quenching curve for immobilized Ru(bpy)₃²⁺ by 5-HT (A) and tyramine (B) in 50 mM PBS at pH = 8.0 containing 0.5 mM TPA. The scan rate was 0.1 V/s.

The reason is that at higher pH value radical cations deprotonate more easily to form high free radical intermediates. However, too high pH led to the decreased amount of Ru(bpy)₃²⁺ due to the competitive reactions with hydroxide ions [38,39]. Therefore 50 mM pH = 8.0 PBS was applied.

3.7. Optimization of separation conditions

The effect of pH of running buffer on the separation efficiency (resolution, Rs) was investigated. As illustrated in Figure S5, the highest quench efficiency was observed at pH = 8.0 and 8.5 for tyramine (circles) and 5-HT (squares), respectively. Considering that the Rs increased with the pH increase from 5.5 to 8.5 and further increase in the pH caused a decrease in Rs (triangles), pH = 8.5 was selected as the running buffer solution. Ionic concentration of the running buffer solution was further examined. The strongest ECL signals and the good Rs obtained when 15 mM PBS were used (Figure S6). Considering higher ionic concentrations led to longer migration times and stronger Joule heating, 15 mM pH = 8.5 PBS was used as the running buffer solution.

3.8. Performance characteristics of the method

The calibration curves were calculated by plotting the peak height values against the analyte concentrations. The ECL intensity varied linearly with its concentrations ranging from 0.1 μM to 100 μM for 5-HT and from 1.0 μM to 80 μM for tyramine. The linear equations and regression coefficients (R)

were $Y = 29.75 X + 525.30$ for 5-HT ($R = 0.9999$) and $Y = 36.98 X + 464.03$ ($R = 0.9986$) for tyramine, where X and Y stood for the concentration of analytes and the corresponding quenched ECL intensity, respectively. Based on an S/N = 3, the limit of detection (LOD) for 5-HT and tyramine were 0.02 μM and 0.1 μM. The relative standard deviations (RSD) of the ECL intensity for six continuous injections of 20 μM 5-HT and tyramine were 3.50 and 3.60%, respectively.

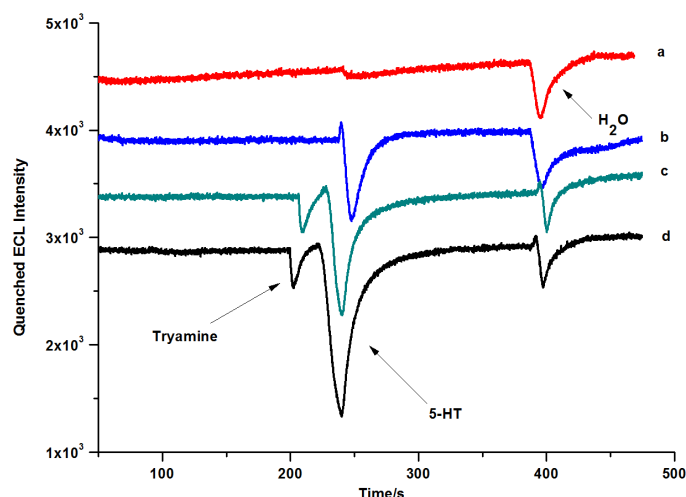
Under the above-mentioned optimum conditions: ECL detection potential of 1.20 V, separation voltage of 15 kV, 50 mM pH = 8.0 PBS in the detection cell, 15 mM pH = 8.5 PBS containing 0.6 mM TPA as the running buffer solution, electrokinetic injection for 10 s at 10 kV, the two analytes were well separated within 500 s. The method was applied to real plasma. Figure 8 (a) and (b) showed electropherograms of the blank solution and patient plasma sample. 5-HT was identified by both the migration time and the spiked method. We added a certain amount of tyramine and 5-HT standard solution to plasma samples. Compared with (b), there has been a new peak in electropherograms of (c), at the same time, the original first peak height increased. We continued to only add 5-HT in sample c, compared with (c), the first peak kept a constant, and the second peak height further increased (d).

Recovery experiments were conducted after spiking plasma samples of small intestine carcinoid with known concentrations of 5-HT and tyramine stock solutions. The results were carried out and listed in Table 1.

The recoveries of 5-HT and tyramine in plasma samples at different concentrations were in the range 81.0-88.8% and 86.1-96.0%, respectively.

Table 1. Recovery for 5-HT and tyramine at different spiked levels in human plasma samples by the proposed CE with quenched ECL method.

Analytes (μM)	Obtained (μM)	Spiked (μM)	Found (μM)	Recovery (%)	RSD (%) (n=3)
5-HT	1.32	1	2.13	81.0	4.0
	1.32	10	10.20	88.8	2.0
	1.32	20	18.85	87.6	2.1
Tyramine		3	2.70	90.1	11.7
		10	9.60	96.0	4.3
		20	17.01	86.1	3.9

**Figure 8.** Electropherograms of (a) H_2O , (b) the extracted human plasma sample, (c) added some tyramine and 5-HT to sample b, and (d) added some 5-HT to sample c. Running buffer: 15 mM PBS at pH = 8.5 containing 0.6 mM TPA; ECL buffer: 50 mM PBS at pH = 8.0 electrokinetic injection: 10 s at 10 kV; separation voltage, 15 kV, detection potential, 1.20 V.

The-HT as an endogenous substance may interact with components in the Plasma during sample processing, resulting in lower recovery. The relative standard deviations (R.S.D.) of ECL peak area was less than 5%, except for the low concentration of tyramine sample.

4. Conclusion

In summary, an efficient immobilized ECL biosensing platform based on $\text{Ru}(\text{bpy})_3^{2+}$ integrated with graphene has been proposed. Coupled with CE method, 5-HT and tyramine were detected based on their quenching effects on the immobilized $\text{Ru}(\text{bpy})_3^{2+}/\text{TPA}$ system. The method displayed a greatly improved sensitivity and simplified compared with static storage mode in which $\text{Ru}(\text{bpy})_3^{2+}$ and TPA solution were simultaneously added to the ECL cell. Thus, this method has the significance to be applied in drug analysis, clinical examination and diagnosis.

Acknowledgments

The project is supported by Natural Science Foundation of Hebei province (B2015201193). Science and Technology Research Project of Hebei Higher Education (QN2016087), Science and Technology Research Program of Baoding City (16ZF190).

Supporting information

The online version of this article contains supplementary material, which is available to authorized users.

Disclosure statement

Conflict of interests: The authors declare that they have no conflict of interest.

Author contributions: All authors contributed equally to this work.

Ethical approval: All ethical guidelines have been adhered.

Sample availability: Samples of the compounds are available from the author.

ORCID

Zi Wei Zhao

 <http://orcid.org/0000-0002-7440-0926>

Fan Lin Li

 <http://orcid.org/0000-0002-7631-5637>

Ming Su

 <http://orcid.org/0000-0002-0874-4958>

References

- [1]. Richter, M. M. *Chem. Rev.* **2004**, *104*, 3003-3036.
- [2]. Richter, M. M.; in: Bard (Eds.), A. J. *Electrogenerated Chemiluminescence*, Marcel Dekker, New York, 2004, 306-308.
- [3]. Fahnrich, K. A.; Pravda, M.; Guilbault, G. G. *Talanta* **2001**, *54*, 531-559.
- [4]. Tokel, N. E.; Bard, A. J. *J. Am. Chem. Soc.* **1972**, *94*, 2862-2863.
- [5]. Deiss, F.; LaFratta, C. N.; Symer, M.; Blicharz, T. M.; Sojic, N.; Walt, D. R. *J. Am. Chem. Soc.* **2009**, *131*, 6088-6089.
- [6]. Van Ingen, H. E.; Chan, D. W.; Hubl, W.; Miyachi, H.; Molina, R.; Pitzel, L.; Ruibal, A.; Rymer, J. C.; Domke, I. *Clin. Chem.* **1998**, *44*, 2530-2536.
- [7]. Tao, Y. W.; Zhang, X. J.; Wang, J. W.; Wang, X. X.; Yang, N. J. *J. Electroanal. Chem.* **2012**, *674*, 65-70.
- [8]. Liu, Y. M.; Cao, J. T.; Zheng, Y. L.; Chen, Y. H. *J. Sep. Sci.* **2008**, *31*, 2463-2469.
- [9]. Pittman, T. L.; Thomson, B. W. *J. Anal. Chim. Acta.* **2009**, *632*, 197-202.
- [10]. Rivera, V. R.; Gamez, F. J.; Keener, W. K.; White, J. A.; Poli, M. A. *Anal. Biochem.* **2006**, *353*, 248-256.
- [11]. Zhang, J.; Qi, H. L.; Li, Y.; Yang, J.; Gao, Q.; Zhang, C. X. *Anal. Chem.* **2008**, *80*, 2888-2894.
- [12]. Su, M.; Wei, W.; Liu, S. Q. *Anal. Chim. Acta.* **2011**, *704*, 16-32.
- [13]. Chen, Y. T.; Lin, Z. Y.; Chen, J. H.; Sun, J. J.; Zhang, L.; Chen, G. N. *J. Chromatogr. A.* **2007**, *1172*, 84-91.
- [14]. Wei, H.; Wang, E. K. *Trends Anal. Chem.* **2008**, *27*, 447-459.
- [15]. Xu, Y. H.; Lou, B. H.; Lv, Z. Z.; Zhou, Z. X.; Zhang, L. B.; Wang, E. K. *Anal. Chim. Acta.* **2013**, *763*, 20-27.

- [16]. Su, M.; Liu, S. Q. *Anal. Biochem.* **2010**, *402*, 1-12.
- [17]. Novoselov, K. S.; Geim, A. K.; Morozov, S. V.; Jiang, D.; Zhang, Y.; Dubonos, S. V.; Grigorieva, I. V.; Firsov, A. A. *Science*. **2004**, *306*, 666-669.
- [18]. Allen, M. J.; Tung, V. C.; Kaner, R. B. *Chem. Rev.* **2010**, *110*, 132-45.
- [19]. Loh, K. P.; Bao, Q.; Eda, G.; Chhowalla, M. *Nat. Chem.* **2010**, *2*, 1015-1024.
- [20]. Li, D.; Müller, M. B.; Gilje, S.; Kaner, R. B.; Wallace, G. G. *Nat. Nanotechnol.* **2008**, *3*, 101-105.
- [21]. Wu, X. M.; Hu, Y. J.; Jin, J.; Zhou, N. L.; Wu, P.; Zhang, H.; Cai, C. X. *Anal. Chem.* **2010**, *82*, 3588-3596.
- [22]. Kovtyukhova, N. I.; Ollivier, P. J.; Martin, B. R.; Mallouk, T. E.; Chizhik, S. A.; Buzaneva, E. V.; Gorchinskiy, A. D. *Chem. Mater.* **1999**, *11*, 771-778.
- [23]. William, S.; Hummers, J. R.; Offeman, R. E. *J. Am. Chem. Soc.* **1958**, *80*, 1339.
- [24]. Wei, W.; Li, D. F.; Pan, X. H.; Liu, S. Q. *Analyst.* **2012**, *137*, 2101-2106.
- [25]. Su, M.; Wei, M.; Zhou, Z. X.; Liu, S. Q. *Biomed. Chromatogr.* **2013**, *27*, 946-952.
- [26]. Wang, D. D.; Li, F. L.; Su, M.; Sun, H. W. *J. Appl. Pharm. Sci.* **2018**, *8*, 007-014.
- [27]. Zhou, M.; Zhai, Y.; Dong, S. *J. Anal. Chem.* **2009**, *81*, 5603-5613.
- [28]. Zhou, M.; Wang, Y.; Zhai, Y.; Zhai, J. F.; Ren, W.; Wang, F.; Dong, S. *J. Chem. Eur. J.* **2009**, *15*, 6116-6120.
- [29]. Schniepp, H. C.; Li, J. L.; McAllister, M. J.; Sai, H.; Margarita, H. A.; Adamson, D. H.; Prud'homme, R. K.; Car, R.; Saville, D. A.; Aksay, I. A. *J. Phys. Chem. B.* **2006**, *110*, 8535-8539.
- [30]. Rillema, D. P.; Jones, D. S.; Levy, H. A. *J. Chem. Soc. Chem. Commun.* **1979**, *19*, 849-851.
- [31]. Karnicka, K.; Miecznikowski, K.; Kowalewska, B.; Skunik, M.; Opallo, M.; Rogalski, J.; Schuhmann, W.; Kulesza, P. *J. Anal. Chem.* **2008**, *80*, 7643-7648.
- [32]. Miao, W. J.; Choi, J. P.; Bard, A. J. *J. Am. Chem. Soc.* **2002**, *124*, 14478-14485.
- [33]. Chi, Y. W.; Dong, Y. Q.; Chen, G. N. *Anal. Chem.* **2007**, *79*, 4521-4528.
- [34]. Heitele, H.; Pöllinger, F.; Kremer, K.; Michel-Beyerle, M. E. *Chem. Phys. Lett.* **1992**, *188*, 270-278.
- [35]. Berthon, R. A.; Colbran, S. B.; Moran, G. M. *Inorg. Chim. Acta.* **1993**, *204*, 3-7.
- [36]. Zheng, H. Z.; Zu, B. *J. Phys. Chem. B* **2005**, *109*, 16047-16051.
- [37]. Zhu, Y. H.; Zhao, B. Y.; Li, L. S. *Anal. Sci.* **2009**, *25*, 785-788.
- [38]. Zorzi, M.; Pastore, P.; Magno, F. *A Anal. Chem.* **2000**, *72*, 4934-4939.
- [39]. Creutz, C.; Sutin, N. *Proc. Nat. Acad. Sci.* **1975**, *72*, 2858-2862.



Copyright © 2019 by Authors. This work is published and licensed by Atlanta Publishing House LLC, Atlanta, GA, USA. The full terms of this license are available at <http://www.eurjchem.com/index.php/eurjchem/pages/view/terms> and incorporate the Creative Commons Attribution-Non Commercial (CC BY NC) (International, v4.0) License (<http://creativecommons.org/licenses/by-nc/4.0>). By accessing the work, you hereby accept the Terms. This is an open access article distributed under the terms and conditions of the CC BY NC License, which permits unrestricted non-commercial use, distribution, and reproduction in any medium, provided the original work is properly cited without any further permission from Atlanta Publishing House LLC (European Journal of Chemistry). No use, distribution or reproduction is permitted which does not comply with these terms. Permissions for commercial use of this work beyond the scope of the License (<http://www.eurjchem.com/index.php/eurjchem/pages/view/terms>) are administered by Atlanta Publishing House LLC (European Journal of Chemistry).